ISSN 1047-8477
Volume 158, Number 1, April 2007

Journal of Structural Biology

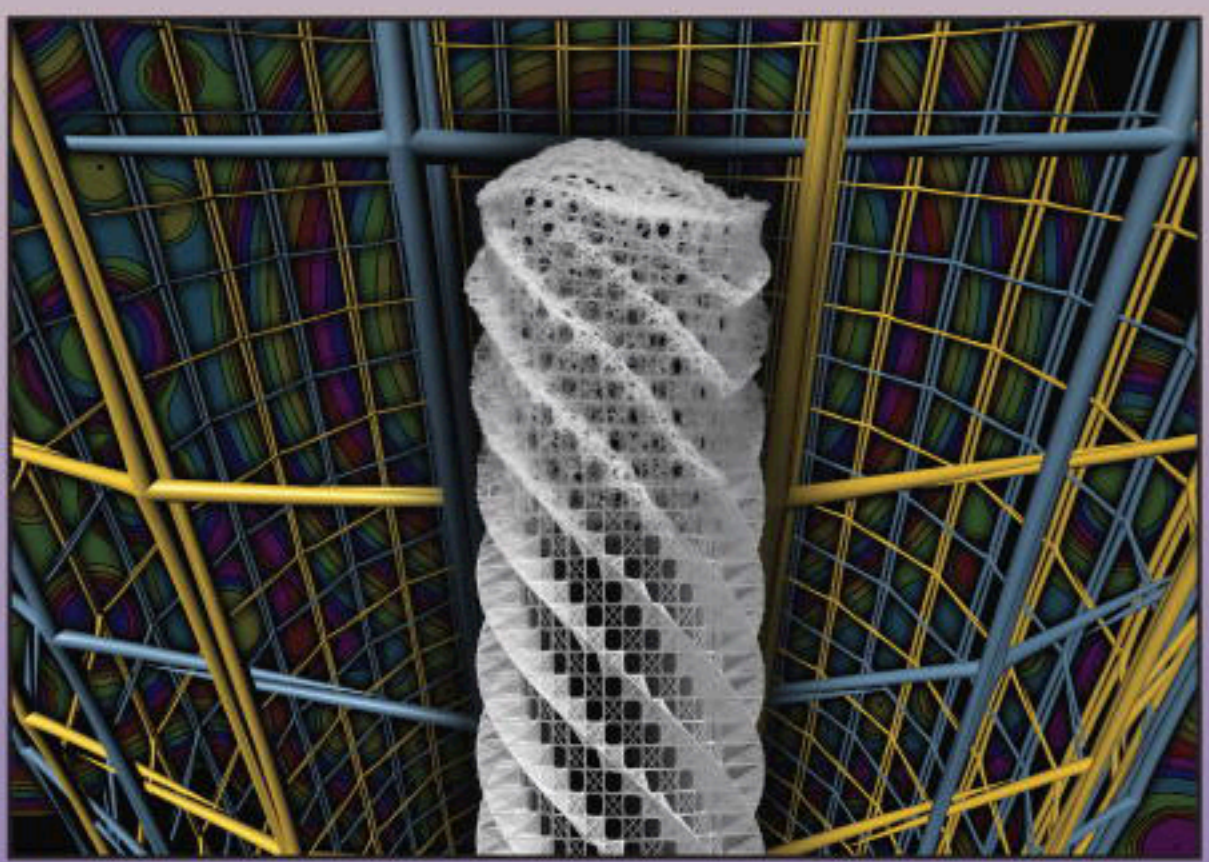

Available online at
ScienceDirect
www.sciencedirect.com

Available online at www.sciencedirect.com
ScienceDirect
Journal of Structural Biology 158 (2007) 93–106
Journal of Structural Biology
www.elsevier.com/locate/yjsbi

Hierarchical assembly of the siliceous skeletal lattice of the hexactinellid sponge *Euplectella aspergillum*

James C. Weaver [a], Joanna Aizenberg [b], Georg E. Fantner [c], David Kisailus [a,1], Alexander Woesz [d], Peter Allen [a], Kirk Fields [e], Michael J. Porter [a], Frank W. Zok [f], Paul K. Hansma [c], Peter Fratzl [d], Daniel E. Morse [a,*]

[a] *Department of Molecular, Cellular and Developmental Biology, Institute for Collaborative Biotechnologies, and the Materials Research Laboratory, University of California, Santa Barbara, CA 93106, USA*
[b] *Bell Laboratories/Lucent Technologies, Murray Hill, NJ 07974, USA*
[c] *Department of Physics, University of California, Santa Barbara, CA 93106, USA*
[d] *Department of Biomaterials, Max-Planck-Institute of Colloids and Interfaces, Potsdam, Germany*
[e] *Department of Mechanical Engineering, University of California, Santa Barbara, CA 93106, USA*
[f] *Materials Department, University of California, Santa Barbara, CA 93106, USA*

Received 22 May 2006; received in revised form 24 October 2006; accepted 25 October 2006
Available online 10 November 2006

Abstract

Despite its inherent mechanical fragility, silica is widely used as a skeletal material in a great diversity of organisms ranging from diatoms and radiolaria to sponges and higher plants. In addition to their micro- and nanoscale structural regularity, many of these hard tissues form complex hierarchically ordered composites. One such example is found in the siliceous skeletal system of the Western Pacific hexactinellid sponge, *Euplectella aspergillum*. In this species, the skeleton comprises an elaborate cylindrical lattice-like structure with at least six hierarchical levels spanning the length scale from nanometers to centimeters. The basic building blocks are laminated skeletal elements (spicules) that consist of a central proteinaceous axial filament surrounded by alternating concentric domains of consolidated silica nanoparticles and organic interlayers. Two intersecting grids of non-planar cruciform spicules define a locally quadrate, globally cylindrical skeletal lattice that provides the framework onto which other skeletal constituents are deposited. The grids are supported by bundles of spicules that form vertical, horizontal and diagonally ordered struts. The overall cylindrical lattice is capped at its upper end by a terminal sieve plate and rooted into the sea floor at its base by a flexible cluster of barbed fibrillar anchor spicules. External diagonally oriented spiral ridges that extend perpendicular to the surface further strengthen the lattice. A secondarily deposited laminated silica matrix that cements the structure together additionally reinforces the resulting skeletal mass. The mechanical consequences of each of these various levels of structural complexity are discussed.
© 2006 Elsevier Inc. All rights reserved.

Keywords: Composite; Toughness; Biosilica; Features; Design; Fibers; Model; Biomimetic; Biomineralization; SEM; Hexactinellida; Spicules

1. Introduction

The hexactinellids are a remarkably diverse and ancient lineage of sponges with a fossil record that dates back more than half a billion years (Gehling and Rigby, 1996; Brasier et al., 1997). Extant members of this sponge class are important contributors to benthic biomass in predominantly deep-sea environments and are frequently found associated with soft sediments. The hexactinellids are characterized by the unique three-axis (six-rayed) symmetry of their skeletal elements (spicules) and their syncytial cellular anatomy (Leys and Lauzon, 1998; Beaulieu, 2001a,b; Janussen et al., 2004). The earliest known

* Corresponding author. Fax: +1 805 893 3416.
E-mail address: d_morse@lifesci.ucsb.edu (D.E. Morse).
[1] Present Address: Sensors and Materials Lab, HRL Laboratories LLC, Malibu, CA 90265, USA.

1047-8477/$ - see front matter © 2006 Elsevier Inc. All rights reserved.
doi:10.1016/j.jsb.2006.10.027

descriptions of hexactinellid skeletal systems in the scientific literature date back to 1780, when spicules from *Dactylocalyx* sp. were described in *Rozier's Journal de Physique*, although at that time, the true biological origin of the examined material was not yet known (Schulze, 1887). Numerous contributions to the fields of hexactinellid anatomy and skeletal morphology were made in the mid 1800s, with studies of specimens from the Challenger expedition of the 1870s being among the most significant (Schulze, 1887). From the examination of living specimens, one could hardly predict the presence of such remarkable skeletal systems as are encountered in members of this unique group of sponges. This is exemplified in the descriptions provided by J.E. Gray in 1872, who stated, "It would be difficult to imagine that the thick, somewhat clumsy, brown tube, perforated with irregular openings, contained any arrangement of support so delicate and symmetrical" (cf. Fig. 1B).

While the elaborate structural complexity of the hexactinellid skeletal systems made them particularly appealing to these early investigators, current research has been aimed at understanding the detailed biosynthetic mechanisms and unique mechanical and optical properties of these remarkable skeletal materials (Cattaneo-Vietti et al., 1996; Levi et al., 1989; Sarikaya et al., 2001). Recently, for example, it was shown that the anchor spicules (basalia) from the Western Pacific sediment dwelling hexactinellid sponge, *Euplectella aspergillum* (Fig. 1A) were comparable to man-made optical fibers in terms of optical properties and superior in terms of fracture resistance (Sundar et al., 2003; Aizenberg et al., 2004). As remarkable as these spicules are, however, they represent only one level of hierarchy in the extremely complex skeletal system of this species (Schulze, 1887; Aizenberg et al., 2005). Recent advances in wide angle and high depth of field scanning electron microscopy have now permitted a reexamination of the early descriptive studies of the skeletal architecture of *E. aspergillum*. Combining an electron micrographic study with three-dimensional structural renderings and design theory, we present here an updated detailed analysis of this complex skeletal system.

2. Materials and methods

2.1. Experimental species

Skeletons of the hexactinellid sponge *E. aspergillum* (of Philippine origin) were examined via SEM, dry in their natural state or following etching with hydrofluoric acid (HF).

2.2. Studies of the native skeleton

Numerous sections (ranging in size from 1×1 cm to 3×3 cm) from various regions of the skeletal lattice were excised with a razor blade and mounted on aluminum disks using either conductive carbon tabs, silver paint, or conductive epoxy, depending on the preferred orientation of the sample being examined.

2.3. Embedding and polishing

5 mm × 1 cm portions of the skeletal lattice were embedded parallel to the long axis of the sponge in M-Bond AE-15 (M-Line, Raleigh, NC) epoxy, sliced into 3 mm thick sections using a diamond cutting wheel, and polished using diamond lapping films down to 0.1 μm grit size under a

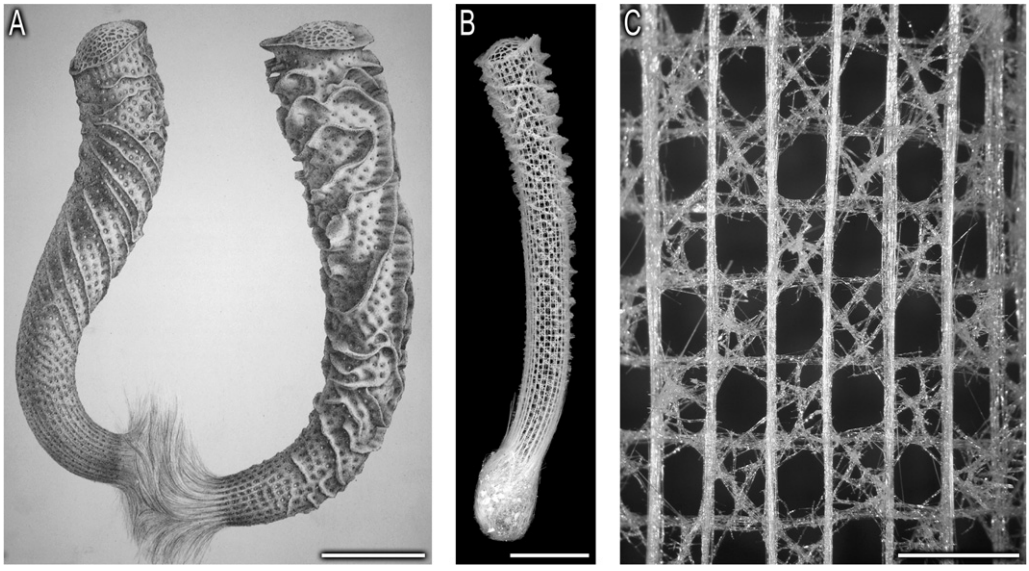

Fig. 1. Details of the Western Pacific hexactinellid sponge, *Euplectella aspergillum*, and its skeleton. (A) Illustration (from Schulze, 1887) of two preserved specimens, clearly showing the holdfast apparatuses, the external ridge systems, and the terminal sieve plates. (B) Photograph of the underlying siliceous cylindrical skeletal lattice exposed by removal of the organic material. (C) At higher magnification, the square-grid architecture and regular ordering of the vertical and horizontal components of the skeletal system are clearly visible. Scale bars: A: 5 cm; B: 5 cm; C: 5 mm.

constant flow of fresh water. Following polishing, the samples were secured to aluminum pin mounts using conductive carbon tape.

2.4. Scanning electron microscopy (SEM)

Following mounting, all samples were sputter-coated with gold and examined with a Tescan Vega TS 5130MM (Brno, Czech Republic) scanning electron microscope. The unique magnetic lens configurations of this microscope permit unusually large field diameters and ultra-high depth of field imaging. Previous attempts to examine the *E. aspergillum* skeletal lattice using traditional SEMs proved unsuccessful, as the inability to examine specimens at low magnifications (less than 50 ×) prevented the clear depiction of large-scale structural features. Due to the transparency of the skeletal system, optical microscopy in many instances was not a viable alternative.

2.5. Atomic force microscopy (AFM)

Embedded samples, describe above, were imaged with a MultiMode AFM system equipped with a Nanoscope 3a controller (Veeco Metrology, Santa Barbara, CA). Images were taken in tapping mode in air with a TAP300 cantilever (Veeco Probes, Santa Barbara, CA) with a nominal spring constant of ~40 N/m and nominal resonance frequency of ~300 kHz. To determine the thickness of the spicule organic interlayers, two different types of samples were examined. In one case, samples were imaged in their native state; in the other, samples were etched for 30 s in 500 mM NH_4F:250 mM HF to reveal the locations of the organic interlayers. Line scan profiles through 10 images of each sample type were used to calculate interlayer thickness.

2.6. Three-dimensional structural renderings

Because of the structural complexity of the *E. aspergillum* skeletal system, the generation of three-dimensional models was necessary to clearly depict the various design elements present and the various stages of skeletal maturation. These models were constructed using information obtained from scanning electron and optical microscopy studies of (1) native, (2) partially demineralized, (3) fractured, (4) sectioned and (5) crushed examples of the *E. aspergillum* skeletal lattice and were compiled using the three dimensional structural rendering program, Maya 6.0 (Alias; Toronto, Canada). For the structural rendering work, more than 50 different specimens were examined in order to elucidate the general design principles used in skeletal construction; the images provided are representative of the results we obtained.

3. Results and discussion

Using modern advances in electron microscopy and three-dimensional structural rendering, we have combined our observations with Schulze's original descriptions of *E. aspergillum* collected during the Challenger expedition between 1873 and 1876, in an attempt to update and unify the already impressive coverage of the individual design elements present. The main levels of structural hierarchy, which range in dimensions from 10s of nm to 10s of cm, are summarized in Fig. 2 and described in detail below. Briefly, in this skeletal system, organic and inorganic components assemble to form a composite spicule structure. Non-planar cruciform spicules are organized to form a three-dimensional cylindrical network. The walls of the resulting structure are cemented and strengthened by spicule bundles, oriented vertically, horizontally and diagonally with respect to the cylindrical lattice. At a coarser scale, spicules are arranged to form a series of diagonal (helical) ridges on the external wall of the lattice. The entire configuration is cemented by additional silica-rich composite layers. The structural components and their mechanical contributions to the bulk skeletal lattice that exist at each hierarchical level are described below.

3.1. Axial filament

The organic scaffold onto which silica is deposited consists of a central proteinaceous axial filament that exhibits a distinctly square or rectangular cross-section (Fig. 3A) (Reiswig and Mackie, 1983). This is in stark contrast to the pseudohexagonal cross-sectional morphology characteristic of demosponge axial filaments (Garrone, 1969), the biochemistry and histology of which have been heavily investigated (Simpson et al., 1985; Shimizu et al., 1998; Cha et al., 1999; Zhou et al., 1999; Krasko et al., 2000; Pozzolini et al., 2004; Muller et al., 2005; Murr and Morse, 2005; Schröder et al., 2006). In demosponges, these axial filaments have been demonstrated *in vitro* to catalyze the hydrolysis and polycondensation of silicon alkoxides and related molecular precursors to form silica at ambient temperature and pressure and near neutral pH, and to serve as templates for the deposition of the silica. These observations suggest that the axial filaments and their constituent globular enzymatic proteins, the silicateins, may play a critical role *in vivo* in the initial induction of silica deposition during spicule formation (Morse, 1999, 2000; Shimizu and Morse, 2000; Sumerel and Morse, 2003). Based on the fact that both demosponge and hexactinellid spicules contain proteinaceous axial filaments, it is expected that both might exhibit similar catalytic and templating activities. It is important to note, however, that preliminary X-ray diffraction studies of demosponge and hexactinellid axial filaments reveal that the packing arrangements of the constituent proteins are fundamentally different (Croce et al., 2004). These observations suggest the possibility that the proteins themselves may also be structurally distinct from one another. Preliminary SDS–PAGE analyses support this suggestion (Weaver and Morse, 2003).

Moreover, the fundamental mechanisms by which spicule growth occurs are distinctly different in these two

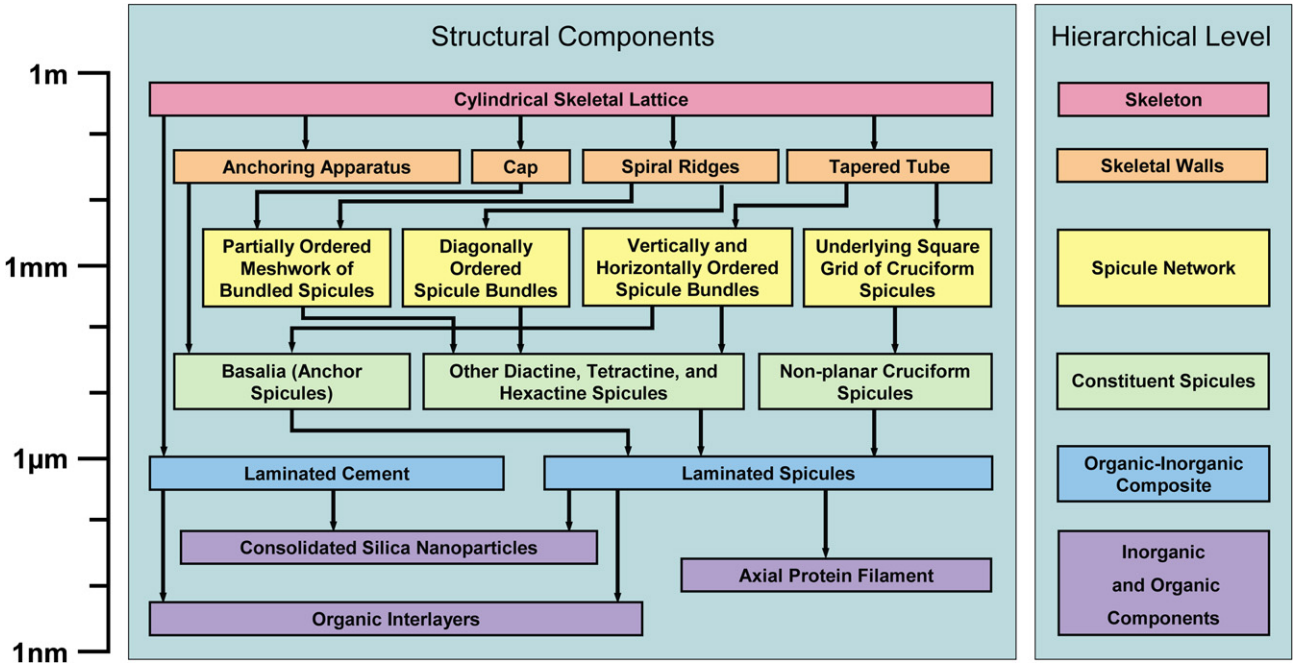

Fig. 2. Schematic representation of the hierarchical levels (right) of organization in the *Euplectella aspergillum* skeletal lattice and the individual structural components (left). The levels of complexity increase with the length scale. The arrows indicate the component parts of each successively more complex structural level.

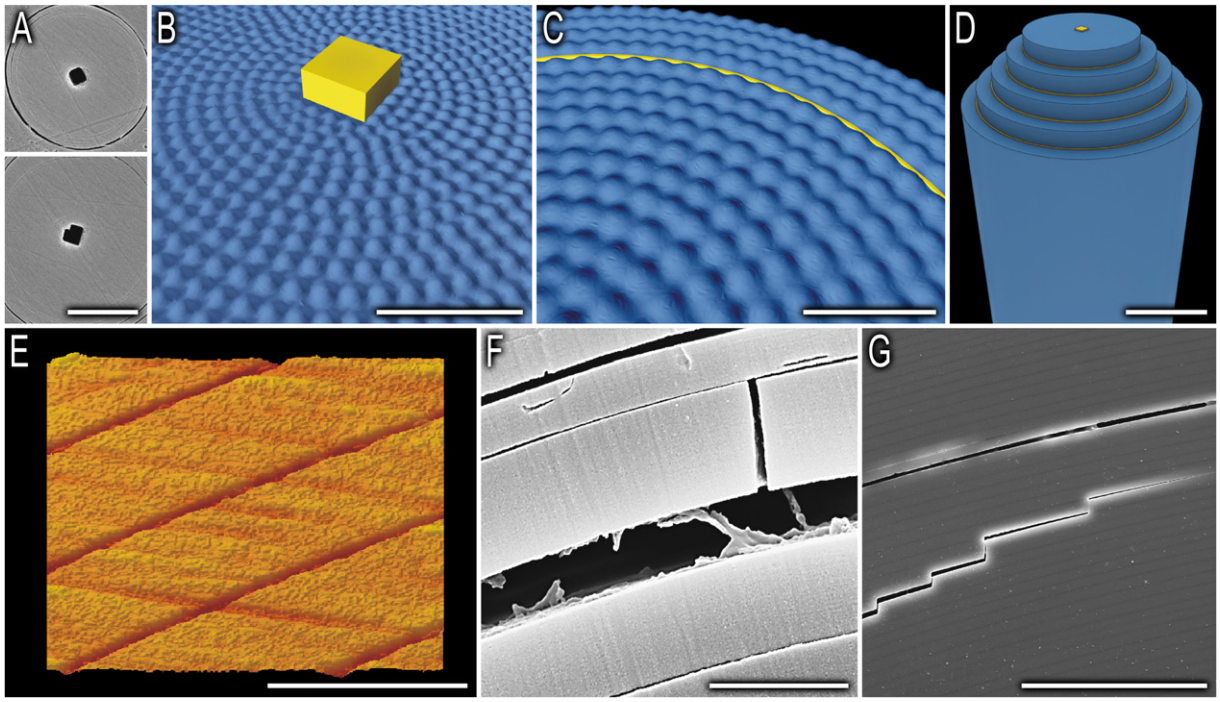

Fig. 3. Laminated organic/inorganic hybrid structure of the spicules. (A) Scanning electron micrographs of polished spicule specimens reveal the square cross-section of the central proteinaceous axial filament upon which concentric lamellae of consolidated silica nanoparticles are deposited; B–D: Three-dimensional structural renderings of the silica/protein hybrid, depicting the central or axial silica cylinder of the spicule deposited around the axial filament (B), organic interlayers (shown in yellow) deposited throughout the cortex of the spicule (C), and the resulting laminated organic–inorganic composite structure (D). (E) AFM reveals that each of these organic layers measures only 5–10 nm in thickness. (F) Scanning electron micrograph showing individual layers revealed during spicule failure. When stressed mechanically, a propagating crack exhibits a distinct stepped architecture as the organic layers induce lateral crack deflection, clearly shown in the scanning electron micrograph from a related species in (G). Scale bars: A: 2.5 μm; B: 1 μm; C: 500 nm; D: 5 μm; E: 500 nm; F: 500 nm; G: 50 μm.

sponge classes. In demosponges, recent evidence suggests that the axial filament is synthesized in its entirety prior to silica deposition (Uriz et al., 2000): the maximum spicule dimensions thus being predetermined by the length of the axial filament. In contrast, during spicule growth in hexactinellids, the axial filament appears to be connected to the surrounding syncytium through an opening at the end of each ray. After the ray has ceased to grow in length, the terminal opening is closed by an expansion of the silica layers (Schulze, 1887). In addition to these observations in mature specimens, this growth mode also has been suggested from observations of the early stages of spicule biosynthesis in larvae of the hexactinellid, *Oopsacas minuta* (Leys, 2003). These data help explain how hexactinellids are able to synthesize the unusually long spicules that are so commonly observed in members of this sponge class (Simpson, 1984; Levi et al., 1989). It is equally important to note that the remarkable size of hexactinellid spicules is also permitted by (and may be the direct result of) their syncytial architecture at the cellular level (Mackie and Singla, 1983). The polynucleate nature of the syncytial sclerocytes (the cells in which mineralization occurs) facilitates their potential extension across the entire length of the living sponge, thus permitting the synthesis of equally long skeletal elements.

3.2. Consolidated silica nanoparticles

The silica deposited around the proteinaceous axial filament consists of consolidated silica nanoparticles measuring between 50 and 200 nm in diameter (Aizenberg et al., 2004, 2005). The nanoparticles are continually deposited in discrete concentric layers during spicule growth (Fig. 3B and C), with a gradual increase in mean particle size from the spicule interior to the outer cortex.[2a] It is important to note that these nanoparticles are only visible by SEM following etching with either sodium hypochlorite or HF. Recent small-angle X-ray diffraction studies of the spicule silica reveals that these 50–200 nm diameter particles are themselves composed of even smaller 3 nm diameter particles (Woesz et al., 2006). The resulting silica exhibits an initial elastic modulus that is approximately half that of technical quartz glass (Woesz et al., 2006), the values for which are in close agreement with those reported from other hexactinellids (Levi et al., 1989).

From a structural perspective, the silica behaves the same as homogeneous bulk silica; for instance, fracture surfaces are essentially planar and featureless in both. The presence of silica nanoparticles in these spicules, like those from demosponges (Weaver et al., 2003), is not unexpected, as this is the most kinetically favored form of silica deposited from solution (Iler, 1979). Similar structural motifs have been observed in other silicifying taxa such as diatoms (Crawford et al., 2001; Noll et al., 2002), and in the *in vitro* formation of silica catalyzed and templated by the silicatein filaments from a demosponge (Cha et al., 1999).

3.3. Laminated spicule structure consisting of alternating layers of silica and organic material

The innermost mineralized portion immediately surrounding the axial filament, the central or axial cylinder, is generally distinguishable from the layered outer cortex by the absence of lamination and appears in fractured spicules as a featureless solid cylinder of hydrated silica (Fig. 3A and B). Surrounding this central cylinder is the spicule cortex, which exhibits a distinctly laminated architecture (Fig. 3C and D) (Schulze, 1887). From the behavior of the spicules when heated, and when examined in polarized light, Schultze, in 1860, determined that the individual lamellae are separated from one another by thin organic layers. Despite this significant early discovery, the validity of these observations has been continuously questioned in the scientific literature (Schulze, 1925; Schmidt, 1926; Travis et al., 1967; Jones, 1979; Simpson, 1984) and has been only recently confirmed by high-resolution secondary

[2] Because the specimens examined exhibited extensive variability in size, extent of development, and mineralization, the mean values for dimensions of structural features (averaged over many specimens) do not necessarily reflect the architectural regularity seen in each specimen. The following useful dimensional parameters can be extracted and generalized for this species: (a) *Spicule silica particle size.* We observe a progressive increase in mean particle diameter from the central cylinder of silica to the outer laminated cortex (Aizenberg et al., 2004). Particle size averages 48 ± 9 nm ($n = 100$) in the central cylinder and gradually increases to 187 ± 34 nm ($n = 100$) in the outer cortex. (b) *Stauractine silica layer thickness.* There is a gradual increase in silica layer thickness within the main cruciform load bearing (stauractine) spicules. Silica layer thickness increases by an average of 7.0-fold ± 2.9-fold ($n = 10$) from the outermost to the innermost layers. (c) *Bulk dimensions of the skeletal lattice.* While there exists extensive intraspecific variability in the size of specimens examined in this study, on average, the diameters of specimens examined increase by 1.7-fold ± 0.22-fold ($n = 20$) from the bottom (point of holdfast attachment) to the top (site of the terminal sieve plate) of the lattice. (d) *Sizes of rectangular openings in the skeletal lattice.* The center-to-center spacing between the struts defining the rectangular openings is approximately 1/36 of the tube circumference at a prescribed axial location. The width of the openings is only slightly smaller: the difference being the thickness of the intervening struts (Fig. 5). The width of each rectangular opening within a given region of the skeletal lattice varies on average by only ±6.1% ($n = 20$). (e) *Vertical and horizontal strut dimensions.* Diameters of the reinforcing struts vary significantly from specimen to specimen, depending on the degree of skeletal mineralization (rather than location). Within a given specimen these diameters are relatively consistent, varying only by an average of ±17% ($n = 20$). (f) *Ridge height.* While ridge height varies as a function of specimen size and the degree of total skeletal mineralization, ridge height increases linearly from the bottom to the top of the skeletal lattice on average by 5.3-fold ± 1.5-fold ($n = 20$). (g) *Average or representative structure.* Using the above criteria and the median values presented in the previous sections, we can reconstruct a hypothetical representative sponge skeleton exhibiting the following dimensions: The representative skeleton would measure ca. 25 cm in height and increase slowly in diameter from 2.5 cm at its base to ca. 4.25 ± 0.94 cm at its apex. There would be ca. 36 vertical and 70 horizontal spicular struts. The average width of these reinforcing struts would measure ca. 350 ± 60 μm, and the resulting rectangular openings in the skeletal lattice would measure, center to center, 2.18 ± 0.13 mm in the lower regions of the skeletal lattice and ca. 3.7 ± 0.22 mm near the apex. Ridge height would slowly increase from 1.13 mm at its base to 6 ± 1.7 mm near the apex.

and backscattered electron microscopy and Raman spectroscopic imaging (Aizenberg et al., 2005; Woesz et al., 2006). These organic layers (Fig. 3F) are on the order of ca. 5–10 nm thick, as measured by AFM of spicule cross-sections (Fig. 3E). With the intervening silica layers being 0.1–2.0 μm thick, the volume fraction of the organic phase is small: typically <1% (cf. below).

This laminated design is critical for imparting damage tolerance to the individual spicules and the overall skeletal structure (Seshadri et al., 2002; Chai and Lawn, 2002). Provided that the organic interlayers are sufficiently weak, cracks propagating through the silica layers are arrested and deflected along the interlayer boundary. Consequently, rather than failing catastrophically, the spicules fracture through a series of successive crack arrest, re-nucleation and discrete propagation events (Fig. 3G). In contrast, monolithic silica fibers fail by the propagation of a single dominant flaw.

When examined in cross-section, it becomes readily apparent that silica layer thickness does not remain constant within the cortical region of the spicule. Instead, these layers gradually decrease in thickness from the central cylinder to the spicule periphery.[2b] During mechanical loading, the thin outer layers fracture first, resulting in the dissipation of large quantities of energy primarily via the spreading of cracks through the delamination of the silica layers at the organic–inorganic interface. These thinner layers also significantly limit the depth of crack penetration into the spicule interior.

At the macroscopic level, the majority of hexactinellid spicules exhibit a unifying design strategy regardless of the number of rays present. This homogeneity of design is a hallmark of the Hexactinellida, despite the remarkable structural diversity of spicules observed in this group. Recognized by numerous authors in the mid 1800s, the presence of three equal axes intersecting at right angles is the fundamental structure of all hexactinellid skeletal elements, and relates to both those spicules united into a continuous framework, and those which lie isolated in the syncytium.

The deviations from this general design strategy include the following modifications: (l) unequal development of the rays, including the complete suppression of one or more, so that in extreme cases only a single ray attains full development, (2) division of the rays into terminal branches, varying in number, form, and direction, (3) the development of local thickenings or unilateral swellings in the form of knobs, thorns, prickles, knots, and similar ornamental protuberances, and (4) the curvature of the chief rays or their branches (from Schulze, 1887). As seen in the next level of structural hierarchy, this design strategy is critical for the establishment of the basic square lattice symmetry of the skeletal system.

3.4. Formation of the underlying quadrate skeletal lattice from non-planar cruciform spicules

Initial surveys of the skeletal lattice suggest that it is principally composed of a series of overlapping vertical, horizontal and diagonal fibrous struts, forming a basic square lattice reinforced with diagonal braces (Fig. 1C). A more detailed examination reveals that the vertical and horizontal struts are significantly more ordered than the diagonal ones, suggesting fundamental differences in the origins of ordering and their dependencies on the underlying constituent spicule geometry. Indeed, the underlying quadrate lattice is principally composed of a network of non-planar cruciform (stauractine) spicules (Fig. 4A–C), with one of the horizontal rays inclined at approximately 20° to the plane of the other three rays.

While their dimensions are somewhat variable, in general the vertical rays are approximately twice the length of the horizontal ones. A generalized spicule schematic is shown in Fig. 4C with vertical rays measuring ca. 10 mm in length and horizontal rays at 5 mm. As seen in Fig. 4B, the base of each spicule ray is between 80 and 100 μm in diameter. The horizontal rays of these spicules overlap with those from a neighboring one and assemble to form the ring-like structures shown in Fig. 4D. Based on this model, the distances between the vertical rays are approximately 5 mm, nearly twice the width of the openings in the skeletal structure (Fig. 1C). Under closer examination, it becomes apparent that the quadrate skeletal lattice is, in reality, composed of two overlapping grid systems: one offset with respect to the other by a distance of half the horizontal ray length. The resulting arrangement, shown in Fig. 4E and F, has openings approximately 2.5 mm wide,[2d] consistent with the experimentally measured values. Higher magnification analyses reveal that all of the vertical components of the grid are positioned on the outside of the lattice and all of the horizontal components on the inside, as seen in the three-dimensional structural rendering (Fig. 4G) and in scanning electron micrographs of the native skeletal lattice (Fig. 4H and I). This organization was first suggested by Schulze in 1887. In his original descriptions, however, Schulze failed to point out the non-planar nature of the cruciform spicules. With planar cruciforms, the interweaving process could only be accomplished by bending of the horizontal rays. The resulting stresses could not be supported during the early stages of skeletal development (prior to the later cementation processes, described below). Moreover, such stresses, if present, would significantly reduce the robustness of the skeletal lattice. Using non-planar spicules, the sponge is able to construct the requisite lattice without introducing internal stresses. Construction of the lattice from cruciform spicules also facilitates growth of the skeletal diameter without changing the number of horizontal struts. Most specimens we examined exhibit a noticeable increase in diameter, from about 2 to 3 cm in the lower portion to 3–5 cm in the upper portion:[2c] the changes occurring smoothly over a length of 20–30 cm (Fig. 5A and B). This is accomplished by varying the degree of overlap between the horizontal rays of the cruciform spicules (Fig. 5C): less overlap results in a greater spacing between the vertical rays and hence a larger cylinder diameter. Since

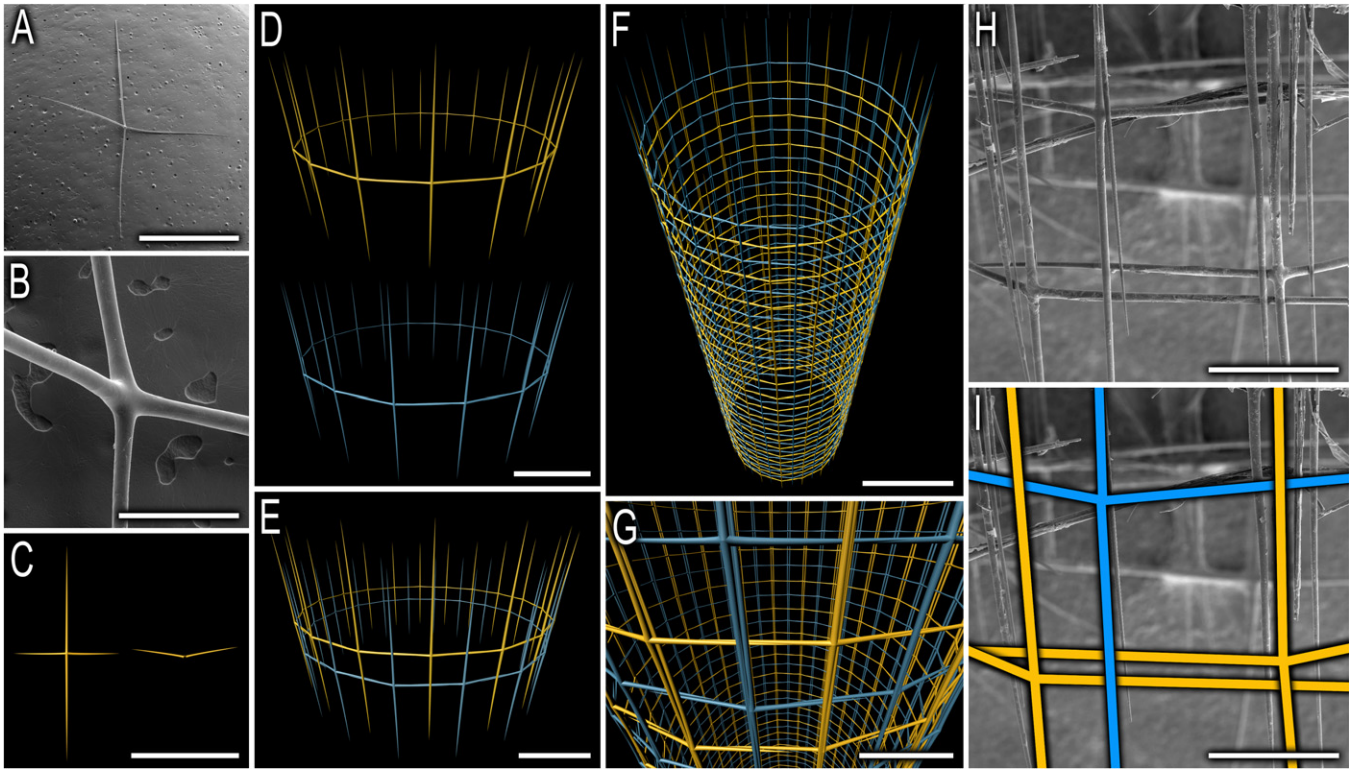

Fig. 4. Steps in the formation of the underlying quadrate skeletal lattice. Scanning electron micrographs of the stauractine (cruciform) spicules from *Euplectella aspergillum* (A, B), clearly show the nonplanar nature of these skeletal elements. Three-dimensional structural renderings depict how the individual spicules (C) assemble to form the ring-like structures shown in (D) by overlap of the horizontal spicule rays. Two separate lattices (shown in blue and yellow) are juxtaposed to form the basic structural unit shown in (E). Further duplication and vertical growth results in the formation of the quadrate lattice shown in (F). Closer examination reveals that due to the 50% horizontal and vertical offset of the two structures, all of the vertical elements become positioned on the exterior of the lattice and the horizontal components on the interior (G). This design strategy can be seen clearly in scanning electron micrographs of a portion of the native skeletal lattice shown in normal (H) and color-enhanced (I) versions. Scale bars: A: 5 mm; B: 500 μm; C: 1 cm; D: 5 mm; E: 5 mm; F: 1 cm; G: 2.5 mm; H: 1 mm; I: 1 mm.

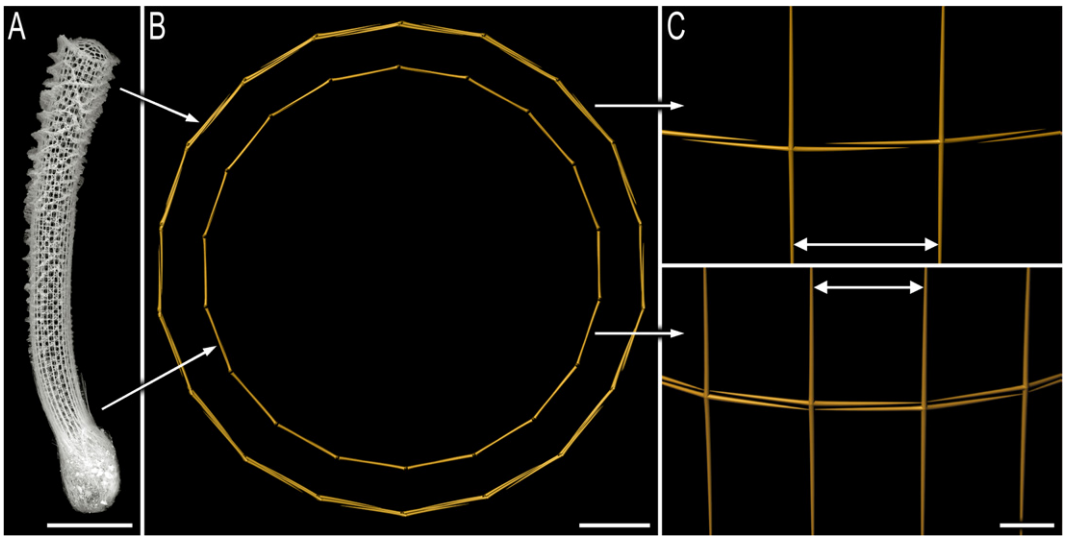

Fig. 5. Factors regulating cross-sectional area of the skeletal lattice. Three-dimensional structural renderings illustrating cross-sections through the upper and lower regions of the skeletal lattice (A) reveal that the numbers of vertical and horizontal components remain constant in these two areas (B). This is accomplished by varying the percent of lateral ray overlap between neighboring spicules (C). Scale bars: A: 5 cm; B: 5 mm; C: 2.5 mm.

the construction of this lattice occurs during the so-called "flexible phase" of sponge growth, these geometric changes can occur without compromising the skeletal symmetry, without inducing large residual stresses, and without the need to synthesize additional skeletal elements. As long as these two distinct lattice systems (shown in blue and

yellow in Fig. 4G) retain their ability to move independently of one another, this design strategy results in the effective division of an applied stress onto two independent strut systems (that are not physically fused to one another). The lack of interconnectivity of this level of design is particularly important in the early stages of synthesis of the skeletal lattice, before secondary reinforcing strategies have yet been implemented.

While fused elements would indeed result in increased stiffness, a consequence of such a rigid design would be decreased strength, as a result of the inability to dissipate energy during substantial loading events. By maintaining a lack of interconnectivity, the structural elements are able to move independently of one another, resulting in a dramatic increase in toughness.

3.5. Vertical and horizontal spicule bundles

Overlaying the quadrate lattice is a series of vertical and horizontal bundled spicular struts between 200 and 500 μm in diameter.[2e] Each consists of a wide size range of individual spicules, ranging from 5 to 50 μm in diameter and of variable length. These struts help stabilize the lattice and provide additional mechanical support (Clegg et al., 1990). This design strategy results in the formation of a series of nearly uniform quadrate meshes averaging 2.5–3 mm in size.[2d] The number of transverse circular spicular struts ranges from sixty to eighty in a full-grown specimen (Schulze, 1887). While the number of vertically oriented struts remains relatively constant along the length of the skeletal lattice, they increase in number by approximately 50% within the upper 2–3 cm due to their occasional splitting. The increase in the number of spicular struts in this region of the sponge may be critical for increasing available surface area for attachment of the terminal sieve plate which covers the entire upper opening of the cylindrical lattice (see Section 3.8 below). The relative locations of these two supporting strut systems are important for further stabilization of the underlying quadrate lattice. In this arrangement, the vertical spicular struts are predominantly arranged on the exterior lattice surface, while the horizontal ones line the interior, with the cruciform spicule grids sandwiched between the two (Fig. 6B). This design strategy increases the toughness of the framework by providing uniform support to the underlying structural framework.

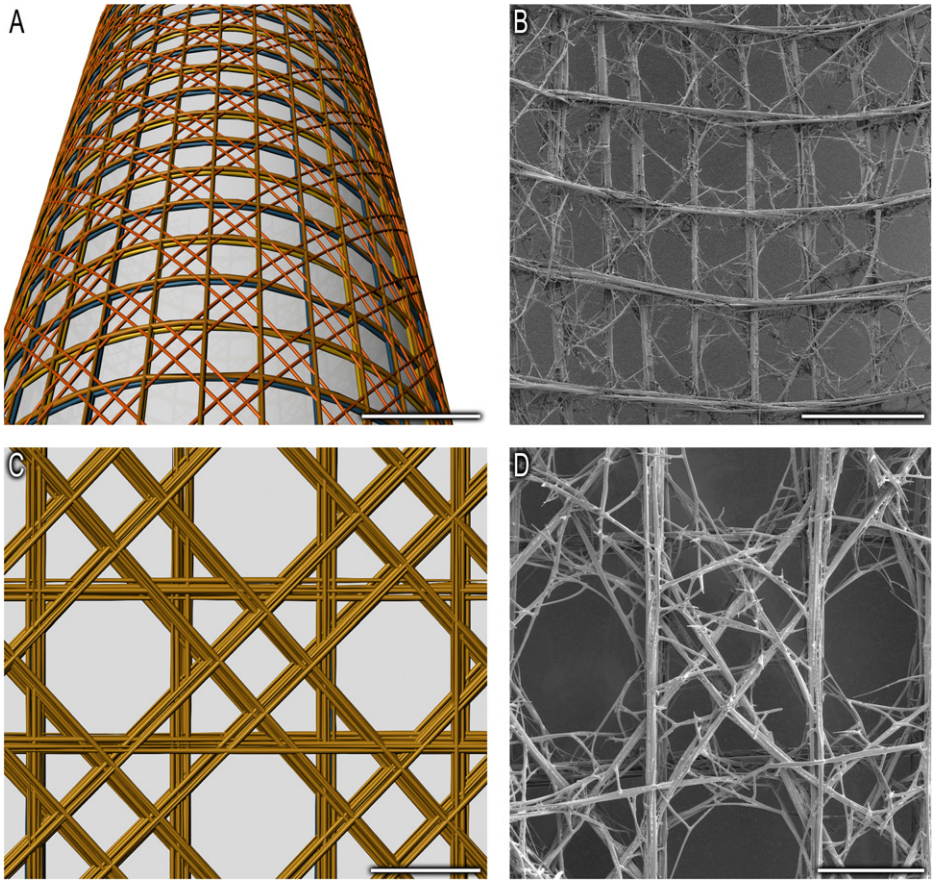

Fig. 6. Vertical, horizontal, and diagonal reinforcement of the cylindrical skeletal lattice. Three-dimensional structural renderings show that superimposed on the underlying quadrate lattice are a series of vertical, horizontal, and diagonal struts, which form an alternating open and closed cell structure (A). Scanning electron micrograph of the interior lattice wall reveals that the horizontal supporting struts are predominantly positioned on the interior lattice surface and the vertical components are on the exterior (B). Each strut is in turn composed of a series of individual spicules bundled together (C). Scanning electron microscopy provides a comparative view of a similar region of the native skeleton showing the semi-disordered nature of the diagonal components (D). Scale bars: A: 5 mm; B: 5 mm; C: 2 mm; D: 2 mm.

The various levels of structural hierarchy discussed thus far are developed during the flexible phase of growth (Saito et al., 2002). It is during this phase that the basic design of the skeletal lattice is formed and square-grid symmetry is established. Since the lattice is easily deformable, it is capable of lateral expansion: a necessity for permitting the three-dimensional growth of the skeletal system. The following structural components are principally designed to reduce flexibility and increase strength as the skeletal lattice matures.

3.6. Diagonal spicule bundles

Outside of the horizontal and vertical struts is an additional set of orthogonal struts, each consisting of similarly bundled spicules, oriented diagonally (at about 45° to the cylinder axis) and surrounding the tube in oblique spirals (Fig. 6A). Each of the spiraling strut systems consists of pairs of parallel spicule bundles, intersecting in a manner that creates a series of alternating open and closed cells, reminiscent of a checkerboard pattern (Fig. 6C and D) (Schulze, 1887). The center to center distance between two adjoining open cells in the same row is, in the upper portions of fully developed specimens, about 6 mm. At the lower end and in young forms, the distance is only 4 mm or less. This alternating open and closed grid cell architecture shares features with the theoretical design criteria for optimized material usage in similar two-dimensional structures subjected to shear stresses (Deshpande et al., 2001; Aizenberg et al., 2005).

While the vertical and horizontal struts precisely follow the contours of the underlying quadrate lattice, the diagonal struts on the other hand do not have such a pre-existing roadmap, as is reflected in their semi-disordered nature. It is important to note that in general, the quantity of material forming each of the diagonal strut systems (organized as right or left handed helices) approximately equals that of the vertical or horizontal components. Thus from the perspective of material consumption, the skeletal system does approximately follow the optimum design strategies described by Deshpande et al. (2001).

The incorporation of diagonal bracings is essential for supporting bending, shear, and torsional loads exerted on the skeletal lattice. The sponge is able to increase strength by reducing the lattice cell area through reinforcement with two sets of partially disordered diagonal strut systems.

This design strategy may also have additional benefits. Since the external ridges are constructed along the diagonal strut systems (as described in the section immediately below), more surface area available for ridge connectivity and support are provided by doubling the number of diagonal structural elements resulting in the formation of a supporting basal grid, without reducing the number of openings available for water filtering. It also is relevant to note that by offsetting the diagonals from the node (Fig. 6C and D), roughly octagonal openings are formed, that may help guide the development and provide support for the water-filtering and current-generating structures of the living tissue.

3.7. External diagonally ordered ridge system

In young specimens, and on the lower portions of older forms, a slightly arched protuberance is formed in the middle of every four openings in the quadrate lattice. By the fusion of these elevations which lie between two adjacent spiral rows, raised bands are formed, which, after further development, become prominent ridges (Fig. 1A). While the arrangement and development of these ridges varies greatly on the walls of the lower portion of the tube, they are always present, albeit only feebly developed (Fig. 10A, left half of image). These ridges gradually increase in height towards the upper end of the skeletal tube. In some specimens they hardly attain a maximum dimension of 2 or 3 mm, while in other cases they extend 10 mm or more[2f] (from Schulze, 1887).

The ridges are supported by a series of steeply set beams which unite at an acute angle corresponding to the sharp edge of the ridges. They are also firmly fused laterally to one another and to the strong latticework of the tube. The beams are crossed both by long spiraling fibers which run parallel to the edge of the ridges and by small short beams which run through the ridges transversely, forming the basic ridge structure shown in Fig. 7A.

Although they run predominantly parallel to the spiral rows of gaps, the ridges seldom continue in the same direction beyond a semirevolution. They often bend around at right angles, at the end of half a spiral turn, and extend in the opposite direction down the other side of the tube (Fig. 7B and C). Sometimes they assume an angular or undulating course and occasionally may even form a well-defined grid-like structure (Schulze, 1887).

A typical failure mechanism of a cylindrical tube is ovalization, i.e., deformation of the cross-section from the original circular shape. The presence of a reinforcing ridge or ridges extending perpendicular to the cylinder wall and wrapped circularly around the primary cylinder tends to prevent this failure mechanism, although allowing failure by torsion. By constructing oblique, helical ridges running in opposite directions, the sponge is able to resist both failure modes (ovalization and torsion).

3.8. Terminal sieve plate

At the apex of the skeletal lattice, the open cylinder is covered with an irregular network-like structure that constitutes the terminal sieve plate (Fig. 8A). At higher magnification, it is readily apparent that this structure results from the incorporation of a wide range of morphologically distinct spicules (Fig. 8B). These spicules include various diactines (2-rayed), tetractine (4-rayed) and hexactine (6-rayed) forms. Anchoring of the terminal sieve plate to the lateral walls of the skeletal lattice is facilitated by the vertical and lateral flaring of the constituent spicules,

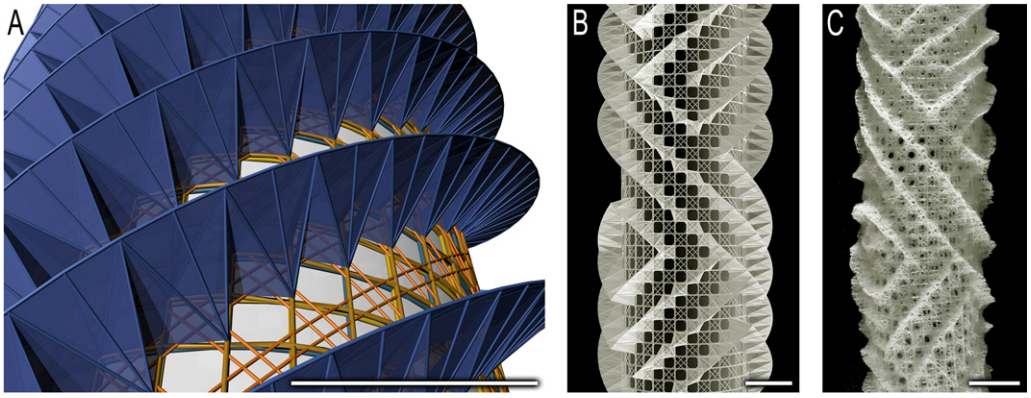

Fig. 7. Structural details of the external spiraling ridges. (A) Three-dimensional structural renderings of the external design elements of the vertical ridge system that spiral around the skeletal lattice. Additional spicules fill in the gaps between the external design elements. (B) The bidirectional ridges occupy a position on every other diagonal set of paired spicular struts. (C) A photograph of the actual specimen after which (B) was modeled. Scale bars: 1 cm.

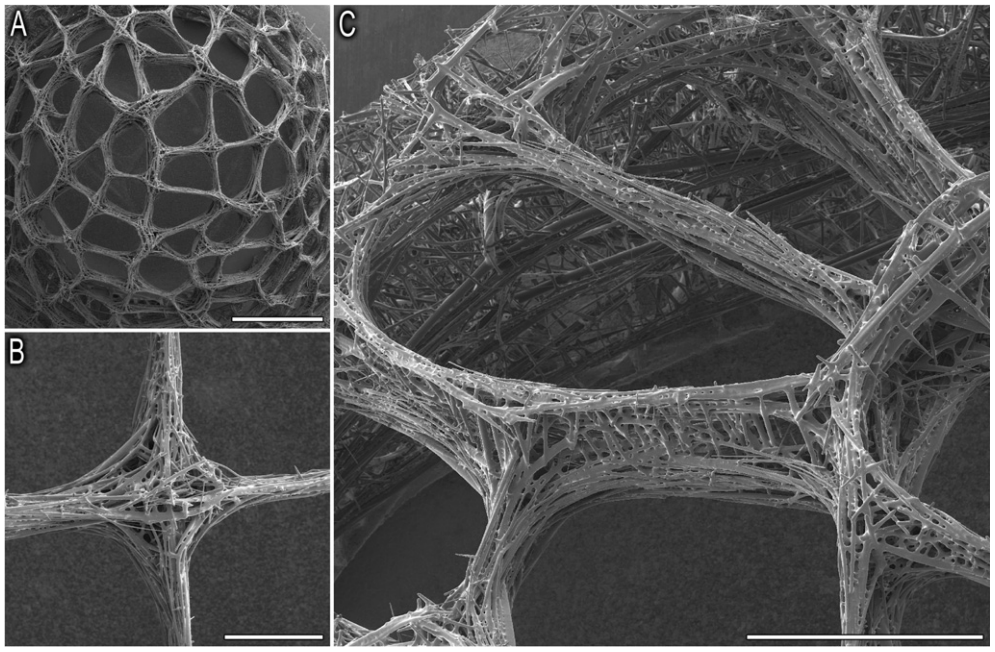

Fig. 8. Organizational detail of the terminal sieve plate. (A) Scanning electron micrograph illustrating the convex nature of the terminal sieve plate. (B) Higher magnification views of this structure reveal that it is composed of a wide range of morphologically distinct spicules cemented together. (C) Lateral and vertical flaring of the peripheral spicules results in complete interdigitation of the sieve plate with the inner wall of the cylindrical skeletal lattice (C). Scale bars: A: 5 mm; B: 1 mm; C: 2 mm.

significantly increasing the available surface area for subsequent structural integration (Fig. 8C).

Bordering the terminal sieve plate is a distinctive ring-like lateral ledge (Fig. 1A). While in many individuals, this structure may be barely visible, it can in others attain a height of 10 mm or more. Usually, however, the "cuff" is not in direct connection with the rest of the ridge system, but is separated from it by a concave circular zone ranging from 5 to 10 mm in width. It is distinguished from the other ridges by being thinner, and typically possessing sharper edges (from Schulze, 1887).

In addition to the ability to protect the sponge interior, the development of a rigid capping structure has important mechanical consequences as well. By preventing lateral collapse of the top of the skeletal lattice, strength and stiffness are significantly increased. Due to the reduced diameter at the base of the skeletal lattice, this secondary reinforcing mechanism may not be necessary in this region for increasing the strength of the bulk composite. While this is the case in most specimens, occasionally a basal sieve plate also may be present (Fig. 9A); it is typically located approximately 1–2 cm above the region at which the anchor spicules become incorporated into the main skeletal lattice. Morphologically, this structure superficially resembles the terminal sieve plate, although it is significantly less developed (Fig. 9B and C). Whether this structure provides additional support in this region of the skeleton is not known. However, its overall rarity, occurring in less than

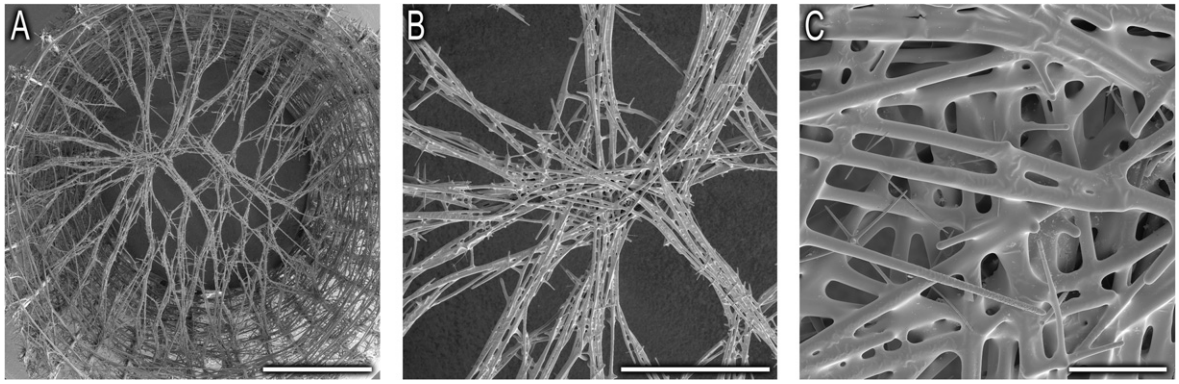

Fig. 9. Scanning electron micrographs of the rare basal sieve plate structure of *Euplectella aspergillum* (A). Higher magnification views of this structure (B, C) suggest a similar design strategy to that observed in the terminal sieve plate. Scale bars: A: 5 mm; B: 2 mm; C: 200 μm.

1% of the specimens we examined, suggests the possibility that it may represent a defect that may develop during skeletogenesis, rather than a functionally significant structure.

3.9. Holdfast apparatus

Superimposed on the reinforced quadrate skeletal lattice in the lower region of the sponge skeleton are bundles of long fibrillar spicules (Fig. 10A). When viewed in cross-section (Fig. 10B), these spicules are easily identifiable. It is these nearly 2000 spicules that go on to form the sponge's anchoring holdfast apparatus (Fig. 1B). The individual spicules (basalia) are shown in the polarized light micrograph in Fig. 10C. Each has a smooth distal and a barbed proximal region that is terminated by an apical spinous process (Fig. 10D) (Aizenberg et al., 2004). This design strategy forms an effective anchoring apparatus that secures the sponge in the soft sediments of the sea floor. The smooth portions of these spicules become incorporated into the main vertical spicular struts of the skeletal lattice and terminate approximately 1/3 of the way up the cylinder.

As has been discussed in the case of plants (Lichtenegger et al., 1999), biology has developed several strategies for anchoring an elongated structure that is subjected to lateral forces. One is the use of structures strong enough to withstand typically encountered lateral forces. This is achieved by a considerable over-strengthening of the anchoring point in order to provide a safety margin sufficient to withstand occasional large forces. A much more economic strategy, also used by young trees (Lichtenegger et al., 1999), is to make the anchoring and/or the rest of the structure sufficiently flexible to allow for significant bending.

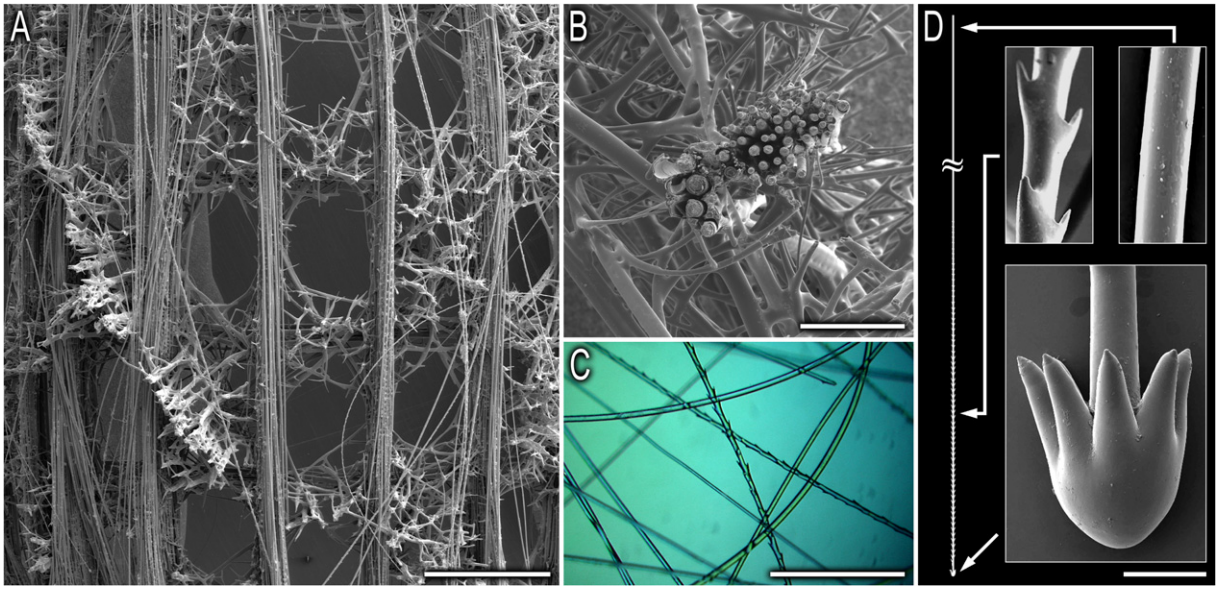

Fig. 10. Organizational and structural features of the holdfast apparatus. Located on the exterior of the spicular strut system near the base of the sponge are, revealed by scanning electron microscopy, a series of bundled fibrillar spicules (A). The spicules are easily seen in a cross-sectional scanning electron micrograph through the lattice in this region (B) and a polarized light micrograph of individual spicules is shown in (C). Scanning electron microscopy reveals that each spicule has a smooth distal region and a barbed proximal region that is terminated by an apical spinous process (D) that is normally buried deep in the sediments. Scale bars: A: 2.5 mm; B: 500 μm; C: 500 μm; D: 100 μm.

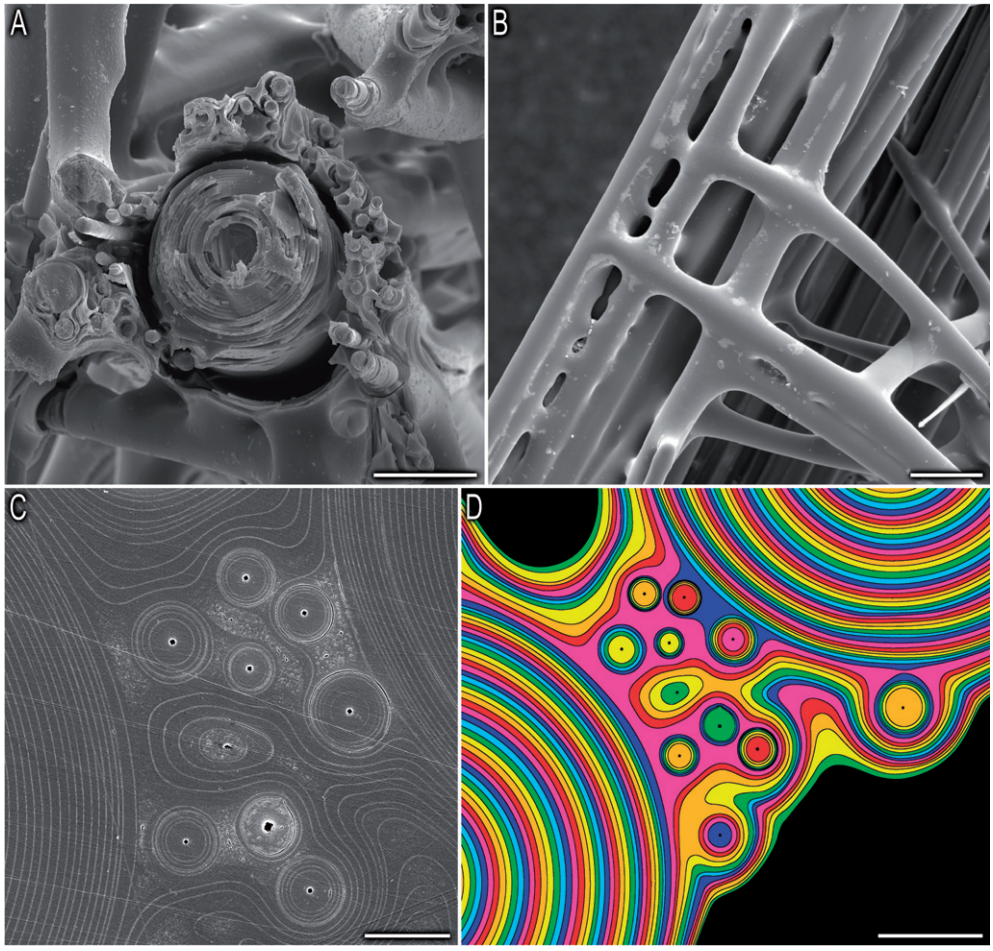

Fig. 11. Organizational details of the consolidating silica matrix. (A) In cross-section, closer examination reveals that surrounding the larger spicules are a network of smaller spicules. (B) An external view of the skeletal lattice's supporting struts reveals the presence of a secondarily deposited silica matrix that surrounds the constituent spicules. (C–D) Polished cross-sections showing the layers of silica cement. Color enhancement of polished cross-sections through a junction of two stauractines (D) reveals the role of the smaller spicules in filling in the gaps between the main load bearing spicules prior to the deposition of the layered silica cement. False colors are used to indicate the various stages of hypersilicification (red first, followed by orange, then yellow, etc.). A scanning electron micrograph of a region of the actual sample depicted in (D) is shown in (C). Scale bars: A: 50 μm; B: 100 μm; C: 10 μm; D: 20 μm.

The latter strategy appears to have been adopted by the sponge, with a flexible anchoring system at a location, which structurally, is the point of highest stress accumulation in the skeletal lattice during lateral loading.

3.10. Consolidation of the entire skeletal lattice with layered silica matrix

In addition to the larger spicules that go on to form the main struts of the skeletal lattice, there are numerous smaller spicules (Fig. 11A), which range from 5–15 μm in diameter. These spicules are embedded in silica matrix that serves as a cement to consolidate and strengthen the entire skeletal system, as seen in cross-sectional micrographs (Fig. 11A) and in external views of the main spicular struts (Fig. 11B). The smaller spicules play a critical role in filling the gaps between the larger spicules, prior to cementation of the skeletal lattice via deposition of multiple layers of silica/organic composite. The use of multiple small spicules cemented as reinforcing filler also can be observed at the junctions of the underlying cruciform spicules (Fig. 11C and D). Examination of these images makes it possible to clearly see the various stages of hypermineralization of this complex skeletal system by visually reconstructing the temporal sequence of cement layer deposition and its subsequent incorporation of the various individual spicules. At higher magnification, it can be seen clearly that the consolidating silica cement precisely follows the contours of the underlying spicules, apparently enhancing the strength of this fiber-reinforced composite, whose structure is similar to armored concrete.

4. Conclusions

Despite the characteristically simple cellular organization of members of the phylum Porifera, it would be incorrect to label the group as "primitive". In many respects, the hierarchical organization of their skeletal

systems is superior to that of even the most complex anthropogenic structures. As described here for *E. aspergillum*, the assembly of the three-dimensional cylindrical skeletal lattice relies on the organized interplay of various components, each of which appears to provide optimum mechanical performance with minimal material use. This biomineralized structure illustrates the nano-, micro-, and macroscale precision that nature employs to construct a wide range of complex yet resilient three-dimensional structures from inherently brittle constituents. Recent attempts at isolation and characterization of the macromolecules involved in biosilicification (Hecky et al., 1973; Harrison, 1996; Shimizu et al., 1998; Cha et al., 1999; Zhou et al., 1999; Carnelli et al., 2001; Kröger et al., 1999, 2000, 2002) have revealed unique and completely unexpected biosynthetic processes, stimulating the development of novel routes to the room temperature synthesis of silicas, siloxanes and metal oxide semiconductors for potential use in a wide range of industrially relevant applications (Parkinson and Gordon, 1999; Vrieling et al., 1999; Morse, 1999, 2001; Cha et al., 2000; Sandhage et al., 2002; Roth et al., 2005; Kisailus et al., 2005a,b, 2006; Schwenzer et al., 2006). By translating the lessons learned from these species to investigations of skeletal fabrication in hexactinellids such as *E. aspergillum*, we come one step closer to not only potentially understanding the selective pressures that resulted in the formation of these remarkable structures, but also new design and synthesis strategies for the next generation of high performance composites.

Acknowledgments

We thank Micha Ilan, Garrett W. Milliron, and Amy Butros for their help and discussions. JCW and DEM were supported by Grants from NASA (NAG1-01-003 and NCC-1-02037), the Institute for Collaborative Biotechnologies through Grant DAAD19-03D-0004 from the Army Research Office, and the NOAA National Sea Grant College Program, U.S. Department of Commerce (NA36RG0537, Project R/MP-92) through the California Sea Grant College System and the MRSEC Program of the National Science Foundation under award# DMR-00-8034 to the UCSB Materials Research Laboratory. GEF and PKH were supported by Grants from National Institutes of Health under Award GM65354, NASA University Research, Engineering and Technology Institute on Bio-inspired Materials under Award No. NCC-1-02037, and a research agreement with Veeco #SB030071. GEF thanks the Austrian Academy of Sciences through a DOC fellowship. JA was supported in part by the Binational US-Israel Science Foundation grant.

References

Aizenberg, J., Sundar, V.C., Yablon, A.D., Weaver, J.C., Chen, G., 2004. Biological glass fibers: Correlation between optical and structural properties. Proc. Natl. Acad. Sci. USA 101, 3358–3363.

Aizenberg, J., Weaver, J.C., Thanawala, M.S., Sundar, V.C., Morse, D.E., Fratzl, P., 2005. Skeleton of *Euplectella*sp.: structural hierarchy from the nanoscale to the macroscale. Science 309, 275–278.

Beaulieu, S.E., 2001a. Colonization of habitat islands in the deep sea: recruitment to glass sponge stalks. Deep-Sea Res. Pt. I 48, 1121–1137.

Beaulieu, S.E., 2001b. Life on glass houses: sponge stalk communities in the deep sea. Mar. Biol. 138, 803–817.

Brasier, M., Green, O., Shields, G., 1997. Ediacarian sponge spicule clusters from southwestern Mongolia and the origin of the Cambrian fauna. Geology 25, 303–306.

Chai, H., Lawn, B.R., 2002. Cracking in brittle laminates from concentrated loads. Acta Mater. 50, 2613–2625.

Carnelli, A.L., Madella, M., Theurillat, J.P., 2001. Biogenic silica production in selected alpine plant species and plant communities. Ann. Bot. London 87, 425–434.

Cha, J.N., Stucky, G.D., Morse, D.E., Deming, T.J., 2000. Biomimetic synthesis of ordered silica structures mediated by block copolypeptides. Nature 403, 289–292.

Crawford, S.A., Higgins, M.J., Mulvaney, P., Wetherbee, R., 2001. Nanostructure of the diatom frustule as revealed by atomic force and scanning electron microscopy. J. Phycol. 37, 543–554.

Clegg, W.J., Kendall, K., Alford, N.M., Button, T.W., Birchall, J.D., 1990. Nature 347, 455–457.

Cattaneo-Vietti, R., Bavestrello, G., Cerrano, C., Sara, M., Benatti, U., Giovine, M., Gaino, E., 1996. Optical fibres in an Antarctic sponge. Nature 383, 397–398.

Cha, J.N., Shimizu, K., Zhou, Y., Christiansen, S.C., Chmelka, B.F., Stucky, G.D., Morse, D.E., 1999. Silicatein filaments and subunits from a marine sponge direct the polymerization of silica and silicones in vitro. Proc. Natl. Acad. Sci. USA 96, 361–365.

Croce, G., Frache, A., Milanesio, M., Marchese, L., Causa, M., Viterbo, D., Barbaglia, A., Bolis, V., Bavestrello, G., Cerrano, C., Benatti, U., Pozzolini, M., Giovine, M., Amenitsch, H., 2004. Structural characterization of siliceous spicules from marine sponges. Biophys. J. 86, 526–534.

Deshpande, V.S., Ashby, M.F., Fleck, N.A., 2001. Foam topology bending versus stretching dominated architectures. Acta Mater. 49, 1035–1040.

Garrone, R., 1969. Collagène, spongine et squelette minèral chez l'èponge *Haliclona rosea* (O.S.) (Dèmosponge, Haplosclèride). J. Microsc. 8, 581–598.

Gray, J.E. 1872. Annals and Magazine of Natural History, ser. 4, vol. IX, 442–461.

Gehling, J.G., Rigby, J.K., 1996. Long expected sponges from the neoproterozoic ediacara fauna of South Australia. J. Paleontol. 2, 185–195.

Harrison, C.C., 1996. Evidence for intramineral macromolecules containing protein from plant silicas. Phytochemistry 41, 37–42.

Hecky, R.E., Mopper, K., Kilham, P., Degens, E.T., 1973. Amino-acid and sugar composition of diatom cell-walls. Mar. Biol. 19, 323–331.

Iler, R.K., 1979. The Chemistry of Silica; Solubility, Polymerization, Colloidal and Surface Properties, and Biochemistry. Wiley and Sons, New York.

Jones, W.C., 1979. The microstructure and genesis of sponge biominerals. In: Levi, C., Boury-Esnault, N. (Eds.), Biologie des Spongiaires, vol. 291. Colloq. Internat, C.N.R.S. Paris, pp. 25–477.

Janussen, D., Tabachnick, K.R., Tendal, O.S., 2004. Deep-sea Hexactinellida (Porifera) of the Weddell Sea. Deep-Sea Res. Part II 51, 1857–1882.

Kröger, N., Deuzmann, R., Sumper, M., 1999. Polycationic peptides from diatom biosilica that direct silica nanosphere formation. Science 286, 1129–1132.

Kröger, N., Deutzmann, R., Bergsdorf, C., Sumper, M., 2000. Species-specific polyamines from diatoms control silica morphology. Proc. Natl. Acad. Sci. USA 97, 14133–14138.

Kröger, N., Lorenz, S., Brunner, E., Sumper, M., 2002. Self-assembly of highly phosphorylated silaffins and their function in biosilica morphogenesis. Science 298, 584–586.

Kisailus, D., Choi, J.H., Weaver, J.C., Yang, W.J., Morse, D.E., 2005a. Enzymatic synthesis and nanostructural control of gallium oxide at low temperature. Adv. Mater. 17, 314–318.

Kisailus, D., Najarian, M., Weaver, J.C., Morse, D.E., 2005b. Functionalized gold nanoparticles mimic catalytic activity of a polysiloxane-synthesizing enzyme. Adv. Mater. 17, 1234–1239.

Kisailus, D., Truong, Q., Amemiya, Y., Weaver, J.C., Morse, D.E., 2006. Self-assembled bifunctional surface mimics an enzymatic and templating protein for the synthesis of a metal oxide semiconductor. Proc. Natl. Acad. Sci. USA 103, 5652–5657.

Krasko, A., Lorenz, B., Batel, R., Schröder, H.C., Müller, I.M., Müller, W.E.G., 2000. Expression of silicatein and collagen genes in the marine sponge *Suberites domuncula* is controlled by silicate and myotrophin. Eur. J. Biochem. 267, 1–11.

Leys, S.P., 2003. Comparative study of spiculogenesis in demosponge and hexactinellid larvae. Microsc. Res. Techn. 62, 300–311.

Leys, S.P., Lauzon, N.R.J., 1998. Hexactinellid sponge ecology: growth rates and seasonality in deep water sponges. J. Exp. Mar. Biol. Ecol. 230, 111–129.

Lichtenegger, H., Reiterer, A., Stanzl-Tschegg, S.E., Fratzl, P., 1999. Variation of cellulose microfibril angles in softwoods and hardwoods—a possible strategy of mechanical optimization. J. Struct. Biol. 128, 257–269.

Levi, C., Barton, J.L., Guillemet, C., Lebras, E., Lehuede, P., 1989. A remarkably strong natural glassy rod—the anchoring spicule of the *Monorhaphis* sponge. J. Mat. Sci. Lett. 8, 337–339.

Morse, D.E., 1999. Silicon biotechnology: harnessing biological silica production to construct new materials. Trends Biotechnol. 17, 230–232.

Morse, D.E., 2000. Silicon biotechnology: proteins, genes and molecular mechanisms controlling biosilica nanofabrication offer new routes to polysiloxane synthesis. In: Auner, N., Weis, J. (Eds.), Organosilicon Chemistry IV: From Molecules to Materials. Wiley-VCH, New York, pp. 5–16.

Morse, D.E., 2001. Biotechnology reveals new routes to synthesis and structural control of silica and polysilsesquioxanes. In: Rappoport, Z., Apeloig, Y. (Eds.), The Chemistry of Organic Silicon Compounds, vol. 3. John Wiley and Sons, New York, pp. 805–819.

Mackie, G.O., Singla, C.L., 1983. Studies on hexactinellid sponges. I. Histology of *Rhabdocalyptus dawsoni* (Lambe, 1873). Phil. Trans. R. Soc. Lond. 301, 365–400.

Murr, M.M., Morse, D.E., 2005. Fractal intermediates in the self-assembly of silicatein filaments. Proc. Natl. Acad. Sci. USA 102, 11657–11662.

Muller, W.E.G., Rothenberger, M., Boreiko, A., Tremel, W., Reiber, A., Schroder, H., 2005. Formation of siliceous spicules in the marine demosponge *Suberites domuncula*. Cell Tissue Res. 321, 285–297.

Noll, F., Sumper, M., Hampp, N., 2002. Nanostructure of diatom silica surfaces and of biomimetic analogues. Nano Lett. 2, 91–95.

Parkinson, J., Gordon, R., 1999. Beyond micromachining: the potential of diatoms. Trends Biotechnol. 17, 190–196.

Pozzolini, M., Sturla, L., Cerrano, C., Bavestrello, G., Camardella, L., Parodi, A.M., Raheli, F., Benatti, U., Muller, W.E.G., Giovine, M., 2004. Molecular cloning of silicatein gene from marine sponge *Petrosia ficiformis* (Porifera, Demospongiae) and development of primmorphs as a model for biosilicification studies. Mar. Biotechnol. 6, 594–603.

Reiswig, H.M., Mackie, G.O., 1983. Studies on Hexactinellid sponges. III. The taxonomic status of Hexactinellida within the porifera. Phil. Trans. R. Soc. Lond. 301, 419–428.

Roth, K.M., Zhou, Y., Yang, W.J., Morse, D.E., 2005. Bifunctional small molecules are biomimetic catalysts for silica synthesis at neutral pH. J. Am. Chem. Soc. 127, 325–330.

Schmidt, W.J., 1926. Uber das wesen der lamellierung und das gegenseitige verhalten von organischer und anorgnischer substanz bei den keiselschwammnadeln. Zool. Zb. Anat. Ont. Tiere. 48, 311–364.

Schulze, F.E., 1887. Report on the Hexactinellida collected by H.M.S. Challenger during the years 1873–1876. Volume XXI.

Schultze, M., 1860. Die Hyalonemen. Bonn: bei Adolph Marcus.

Schulze, P., 1925. Zur morphologischen feinbau der keiselschwammnadeln. Zeit. Morph. Okol. Tiere. 4, 615–625.

Simpson, T.L., 1984. The Cell Biology of Sponges. Springer-Verlag, New York.

Shimizu, K., Morse, D.E., 2000. Biological and biomimetic synthesis of silica and other polysiloxanes. In: Baeuerlein, E. (Ed.), Biomineralization: From Biology to Biotechnology and Medical Application. Wiley-VCH, New York, pp. 207–220.

Sumerel, J.L., Morse, D.E., 2003. Biotechnological advances in biosilicification. In: Müller, W.E. (Ed.), Prog. Molec. Subcellular Biol. 33: Silicon Biomineralization: Biology–Biochemistry–Molecular Biology–Biotechnology. Springer-Verlag, Berlin, pp. 225–247.

Saito, T., Uchida, I., Takeda, M., 2002. Skeletal growth of the deep-sea hexactinelid sponge *Euplectella oweni*, and host selection by the symbiotic shrimp *Spongicola japonica* (Crustacea: Decapoda: Spongicolidae). J. Zool. Lond. 258, 521–529.

Simpson, T.L., Langenbruch, P.F., Scaleraliaci, L., 1985. Silica spicules and axial filaments of the marine sponge *Stelletta grubii* (Porifera, Demospongiae). Zoomorphology 105, 375–382.

Seshadri, M., Bennison, S.J., Jagota, A., Saigal, S., 2002. Mechanical response of cracked laminated plates. Acta Mater. 50, 4477–4490.

Shimizu, K., Cha, J.N., Stucky, G.D., Morse, D.E., 1998. Silicatein α: Cathepsin L-like protein in sponge biosilica. Proc. Natl. Acad. Sci. USA 95, 6234–6238.

Schwenzer, B., Roth, K.M., Gomm, J.R., Murr, M., Morse, D.E., 2006. Kinetically controlled vapor-diffusion synthesis of novel nanostructured metal hydroxide and phosphate films using no organic reagents. J. Mater. Chem. 16, 401–407.

Sundar, V.C., Yablon, A.D., Grazul, J.L., Ilan, M., Aizenberg, J., 2003. Fibre-optical features of a glass sponge—some superior technological secrets have come to light from a deep-sea organism. Nature 424, 899–900.

Sarikaya, M., Fong, H., Sunderland, N., Flinn, B.D., Mayer, G., Mescher, A., Gaino, E., 2001. Biomimetic model of a sponge-spicular optical fiber—mechanical properties and structure. J. Mater. Res. 16, 1420–1428.

Sandhage, K.H., Dickerson, M.B., Huseman, P.M., Caranna, M.A., Clifton, J.D., Bull, T.A., Heibel, T.J., Overton, W.R., Schoenwaelder, M.E.A., 2002. Novel, bioclastic route to self-assembled, 3D, chemically tailored meso/nanostructures: shape-preserving reactive conversion of biosilica (diatom) microshells. Adv. Mater. 14, 429–433.

Schröder, H.C., Boreiko, A., Korzhev, M., Tahir, M.N., Tremel, W., Eckert, C., Ushijima, H., Müller, I.M., Müller, W.E.G., 2006. Co-expression and functional interaction of silicatein with galectin: matrix-guided formation of siliceous spicules in the marine demosponge *suberites domuncula*. J. Biol. chem. 281 (17), 12001–12009.

Travis, D., Francois, C., Bonar, L., Glimcher, M., 1967. Comparative studies of the organic matrices of invertebrate mineralized tissues. J. Ultrastruct. Res. 18, 519–550.

Uriz, M.J., Turon, X., Becerro, M.A., 2000. Silica deposition in Demosponges: Spiculogenesis in *Crambe crambe*. Cell Tissue Res 301, 299–309.

Vrieling, E.G., Beelen, T.P.M., van Santen, R.A., Gieskes, W.W.C., 1999. Diatom silicon biomineralization as an inspirational source of new approaches to silica production. J. Biotechnol. 70, 39–51.

Weaver, J.C., Morse, D.E., 2003. Molecular biology of demosponge axial filaments and their roles in biosilicification. Microsc. Res. Techn. 62, 356–367.

Weaver, J.C., Pietrasanta, L.I., Hedin, N., Chmelka, B.F., Hansma, P.K., Morse, D.E., 2003. Nanostructural features of demosponge biosilica. J. Struct. Biol. 144, 271–281.

Woesz, A., Weaver, J.C., Kazanci, M., Dauphin, Y., Aizenberg, J., Morse, D.E., Fratzl, P., 2006. Micromechanical properties of biological silica in skeletons of deep-sea sponges. J. Mat. Res. 21 (8), 2068–2078.

Zhou, Y., Shimizu, K., Cha, J.N., Stucky, G.D., Morse, D.E., 1999. Efficient catalysis of polysiloxane synthesis by silicatein alpha requires specific hydroxy and imidazole functionalities. Angew. Chem. Int. Ed. 38, 780–782.